ACS APPLIED MATERIALS & INTERFACES

RESEARCH ARTICLE

www.acsami.org

Growth and Morphology of Sputtered Aluminum Thin Films on P3HT Surfaces

Gunar Kaune,[†,‡] Ezzeldin Metwalli,[†] Robert Meier,[†] Volker Körstgens,[†] Kai Schlage,[§] Sebastien Couet,[§,⊥] Ralf Röhlsberger,[§] Stephan V. Roth,[§] and Peter Müller-Buschbaum*[,†]

[†]Technische Universität München, Lehrstuhl für Funktionelle Materialien, Physik-Department E13, James-Franck-Strasse 1, 85747 Garching, Germany

[‡]Martin-Luther-Universität Halle-Wittenberg, von-Danckelmann-Platz 3, 06120 Halle, Germany

[§]HASYLAB at DESY, Notkestrasse 85, 22603 Hamburg, Germany

[⊥]Instituut voor Kern- en Stralingsfysica and INPAC, Celestijnenlaan 200D, K.U. Leuven, B-3001 Leuven, Belgium

ABSTRACT: Growth and morphology of an aluminum (Al) contact on a poly(3-hexylthiophene) (P3HT) thin film are investigated with X-ray methods and related to the interactions at the Al:P3HT interface. Grazing incidence small-angle scattering (GISAXS) is applied in situ during Al sputter deposition to monitor the growth of the layer. A growth mode is found, in which the polymer surface is wetted and rapidly covered with a continuous layer. This growth type results in a homogeneous film without voids and is explained by the strong chemical interaction between Al and P3HT, which suppresses the formation of three-dimensional cluster structures. A corresponding three stage growth model (surface bonding, agglomeration, and layer growth) is derived. X-ray reflectivity shows the penetration of Al atoms into the P3HT film during deposition and the presence of a 2 nm thick intermixing layer at the Al:P3HT interface.

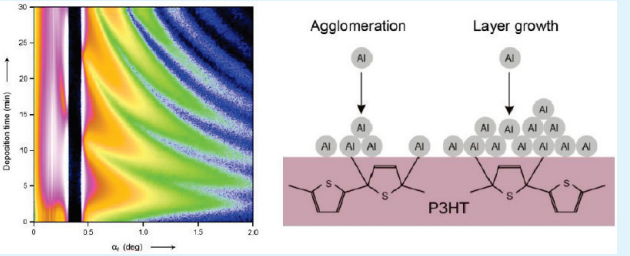

KEYWORDS: aluminum, P3HT, solar cell, GISAXS, sputtering

INTRODUCTION

Thin metal coatings on polymers are an important technological issue and nowadays widely used for decoration purposes, as diffusion barriers in food packaging, or as dielectric layers in microelectronics. Within recent years, a new application for metalized polymer thin films has emerged in the field of organic electronics. Here, a thin metal layer is used to apply electric contact to an electronically active layer such as a conductive polymer or other organic semiconductor. Numerous types of organic field emission transistors (OFET), organic light-emitting diodes (OLED), and organic solar cells (OSC) have already been realized, and most of them use metal contacts to pick up or inject charge carriers.[1−7] Another application is found in tandem or multijunction solar cells, where metallic interlayers serve as charge recombination centers between the single junctions.[8,9]

The performance of these devices crucially depends on the properties of the organic−metal interface. Chemical reactions between metal and organic molecules introduce band gap states and alter the energy level alignment at the interface, resulting in, e.g., inverted contact properties.[10] Depending on the preparation conditions and the reactivity of the involved species, single metal atoms can diffuse into the organic component[11] and act as dopant, which reduces the charge injection barrier or weakens photo luminescence quenching.[12−14] Furthermore, the interface properties determine the adhesion of the metal contact on the active layer and the contact resistance.[15,16] Taking all these points into account, it is obvious that understanding the properties of organic−metal interfaces and their formation processes is of great importance to optimize the characteristics of organic electronic devices.

Historically, the investigation of organic-metal interfaces was driven by the need to achieve proper contact properties of coatings for packaging foils or dielectric layers.[17−20] Later on, the electric properties of organic−metal interfaces came more into focus[10,21−24] and today in particular the relations between the chemical interactions of the involved species and the corresponding interface characteristics are quite well understood.[25−29] However, comparably little work has been done so far on the growth and structural development of metal layers on organic surfaces, although chemical interaction, growth behavior, and interface properties interact all with each other.

Recently, we investigated the growth of a gold contact on a surface of the conducting polymer poly(N-vinylcarbazole). The gold layer growth was followed in situ with grazing incidence small-angle X-ray scattering (GISAXS) during sputter deposition.[30] Because of the low chemical interaction between the two materials, the gold was found to form small spherical clusters on the polymer surface in the initial stage of deposition. By adsorption of incoming gold atoms and under a constant coalescence

Received: December 6, 2010
Accepted: February 14, 2011
Published: March 08, 2011

process, these small clusters grew to larger structures until full surface coverage was reached. Afterward, the gold layer showed a characteristic grain structure that was further coarsened in the continued deposition by grain growth.

In the work presented here, we focus on another material combination which has different interface interactions. The formation of an aluminum (Al) contact on the surface of a poly(3-hexylthiophene) (P3HT) film is probed. Because of its low work function, which matches well the LUMO of P3HT, Al is a common electrode material in P3HT-based organic electronic devices.[3−5] In contrast to the system gold:PVK, the system Al:P3HT is known to be highly reactive. Dannetun et al. extensively studied the interface between aluminum and thiophene semiconductors with spectroscopic methods and found clear proofs for chemical reactions.[21] The formation of Al_2-3T complexes was proposed, where two aluminum atoms covalently bond to every third thiophene ring by splitting up its carbon double bonds.

Resulting from this strong chemical interaction, a constrained growth of the aluminum layer on the P3HT surface can be expected. To study this in detail, a thin layer of aluminum was deposited on a P3HT surface and the layer growth observed in situ with GISAXS. GISAXS is a perfectly suited tool for this kind of investigation, because it can monitor processes in real time and yields broad structural information with nanometer resolution.[31−35] By modeling the 2d GISAXS data the key structural parameters such as thickness, density, and composition of layers or size, shape and spacing of particles at the nanoscale can be extracted.[30,36,37] Related to the deposition conditions, these quantities give the full information about the growth of the deposited layer and its structural evolution.[30]

This article has the following structure: After a description of the investigated samples and a brief introduction to the used experimental methods the resulting morphologies evolving during sputter deposition are presented and discussed. Then the penetration of Al into the polymer film is detailed. The article concludes with a summary of the results and a short outlook.

EXPERIMENTAL SECTION

Sample Preparation. Glass slides were used as substrates and cleaned before coating with the polymer film. For cleaning an acidic bath was applied for 15 min.[38] Poly(3-hexylthiophene) (P3HT) with an average number molecular weight of 16 500 g/mol and a polydispersity of 1.7 was purchased from American Dye Source and dissolved in chloroform in a concentration of 4 mg/mL under permanent stirring. This solution was spin coated with a Süss MicroTec Delta6 RC spin coater under ambient conditions with 2000 rpm for 30 s. The resulting thickness of the P3HT film was determined with X-ray reflectivity to be 42 nm.

GISAXS Measurements and Sputter Deposition. The in situ sputtering GISAXS experiment was performed at the beamline BW4 at HASYLAB (DESY, Hamburg). For this purpose the beamline was equipped with a mobile UHV sputter deposition system, whose details are described elsewhere.[39] The DC magnetron sputtering chamber was operated under an argon pressure of 5×10^{-3} mbar with a power of 6 W. A low deposition rate around 1 nm/min was chosen to accurately control the growth process and to monitor the evolution of the deposited film with high precision. The sample was placed horizontally in the deposition chamber with the surface pointing to the bottom and not heated during deposition. Prior to each deposition step the aluminum target was presputtered for 5 s to remove impurities.

The measurements were done at an X-ray wavelength of 0.138 nm and a sample-to-detector distance of 1.83 m. A setup of high quality entrance slits for precise limitation of the beam divergence in and out of the plane of reflection and a mostly evacuated pathway were used. A moderate microbeam focusing was achieved by using beryllium compound refractive lenses (beam size 60 μm × 30 μm).[40] For the incidence angle, a value of 0.384° well above the critical angle of aluminum was chosen to penetrate the full film. The scattering signal was recorded on a two-dimensional (2d) Pilatus 100K detector with 487 × 195 pixels (172 μm × 172 μm size per pixel) and a low read-out time of 5 ms. In front of the detector, two separate beam stops were installed at the position of the direct beam and the specular peak to shield the detector. Deposition of Al on the polymer film and GISAXS measurement were done continuously without interruption for 30 min. In total 360 images were recorded with an accumulation time of 5 s for each image.

Scanning Electron Microscopy (SEM). SEM images were taken with a field emission SEM (Zeiss NVision 40) operated at an accelerating voltage of 5 kV and at low working distances (WD) from 1.5 to 3 mm.

X-ray Reflectometry. X-ray reflectivity (XRR) data were taken at a Siemens D5000 diffractometer at a wavelength of 0.154 nm ($Cu-K_\alpha$ radiation) in an angular range from 0° to 6° using a Θ-2Θ geometry. A knife edge was used for beam size limitation and background reduction. The reflected intensity was recorded via a point detector. The detector was protected by an automatic beam absorber. The reflectivity data were fitted with a Parratt algorithm to obtain thickness information.

RESULTS

To investigate the growth of an Al contact on top of P3HT, we mounted the initially spin-coated P3HT film in the sputter deposition chamber. First, it was probed without deposition of Al. Al sputtering was then started, and the growth of the Al layer monitored with GISAXS. After 30 min, deposition was stopped and the thickness of the final contact achieved.

The information about the growth process of the layer was extracted from the GISAXS images by modeling and analysis of structural maps. Figure 1a shows seven selected scattering images together with their simulations, which were calculated with the IsGISAXS simulation tool[36] (details see below). In panels b and c in Figure 1 structural maps are shown, which were created by cutting intensity profiles from the scattering images and arranging them with respect to deposition time. These maps provide an overview over the temporal evolution of the scattering images and the deposited layer with the full resolution of the experiment. The cuts were taken at distinct characteristic positions of the GISAXS images. The vertical cuts were taken at $\psi = 0°$, i.e., along the plane of specular reflection, and represent the structure of the layer system perpendicular to the film plane.[31] The horizontal cuts were taken at a constant angle of $\alpha_f = 0.205°$, where aluminum has a maximum in scattering intensity (Yoneda maximum).[41] Thus they are sensitive to structural features in the Al layer and represent its lateral evolution.[31]

The 2d GISAXS data of the uncoated P3HT film (see left image in Figure 1a) show only the Yoneda maxima of glass and P3HT as characteristic signals of the diffuse scattering.[42] The P3HT film exhibits no correlated roughness. Thus no long-ranged correlation between the P3HT film surface and the glass substrate surface is present, which is in contrast to the behavior of nonconducting homopolymer films such as polystyrene (PS) films.[43−45] The absence of correlated roughness might be attributed to the rod-like character of P3HT in contrast to the coil-like one of PS. Because of the increased stiffness of the polymer chain, the substrate roughness is not followed and the polymer surface is statistically independent from the glass surface.

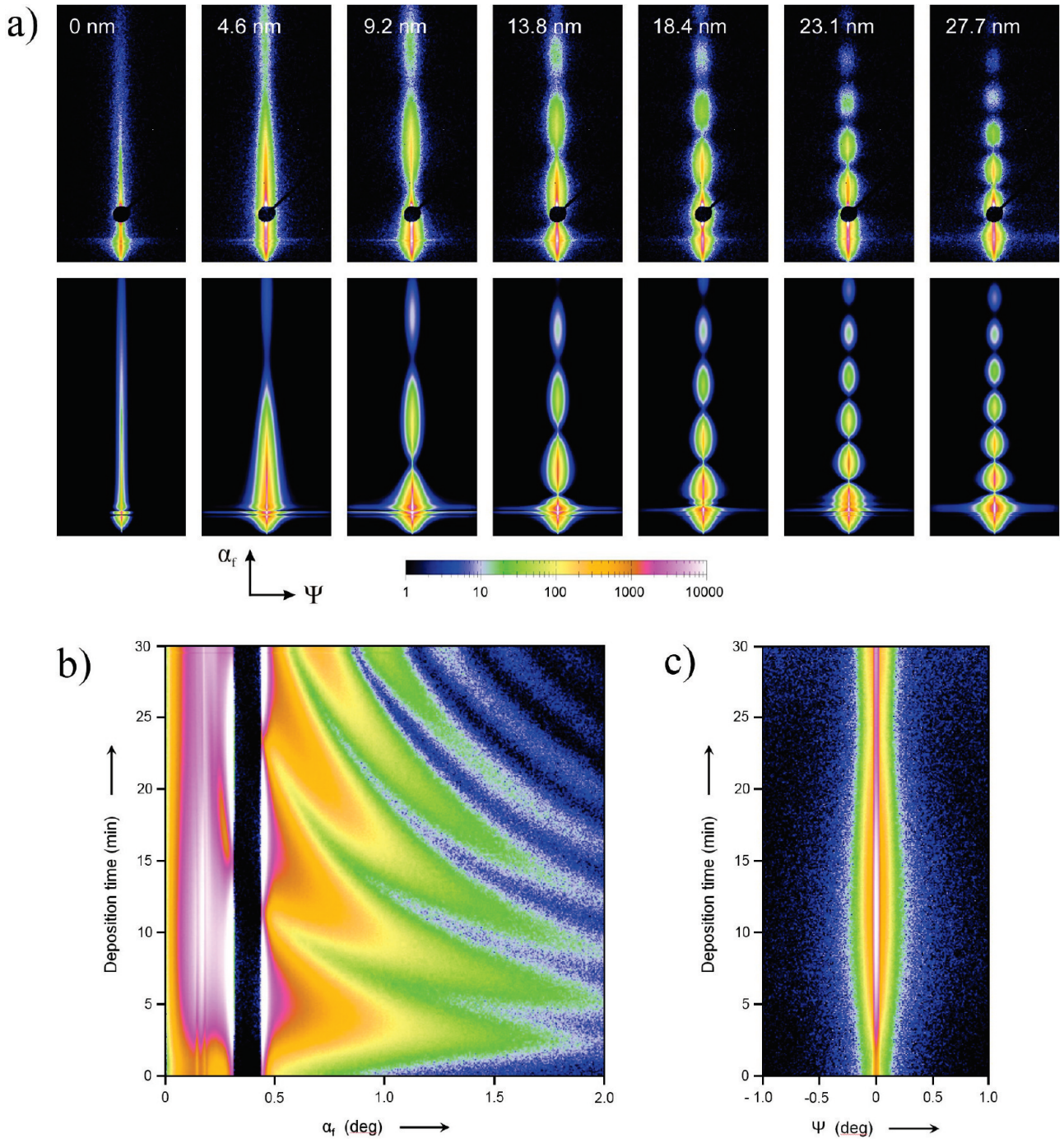

Figure 1. (a) Selected measured and simulated GISAXS images. The measured data (upper row) were taken after deposition times of 0, 5, 10, 15, 20, 25, and 30 min, corresponding to layer thicknesses between 0 nm (uncoated P3HT film) and 27.7 nm. Each image comprises an angular range from 0° to 2° in α_f-direction and from −1° to 1° in ψ-direction. The dark spot in the middle of the images is a beam stop at the position of the specular reflected beam to shield the detector. (b) Structural map created from vertical cuts through the scattering images. Each line is a vertical cut through one image drawn along the plane of reflection (ψ = 0°). (c) Structural map created from horizontal cuts through the scattering images. Each line is a horizontal cut drawn at the position of the Yoneda scattering maximum of aluminum (α_f = 0.205°).

Because of Al deposition on the P3HT, the GISAXS pattern is markedly altered. In the vertical direction, along the α_f-axis, the scattered intensity is modulated with pronounced minima and maxima (see Figure 1a). The map created from the vertical cuts (see Figure 1b) shows this in more detail. Up to a deposition time of 2 min only the scattered intensity increases due to the scattering contribution of the Al deposit. Then, with the formation of a compact Al layer, a modulation begins to develop. This modulation results from a height correlation of the layer with the P3HT surface and describes the layer thickness.[46−48] Thus the Al film exhibits correlated roughness. With ongoing deposition the modulation length decreases as the thickness of the Al layer increases. The pronounced shape of the maxima indicates a homogeneous Al film without large thickness deviations and a

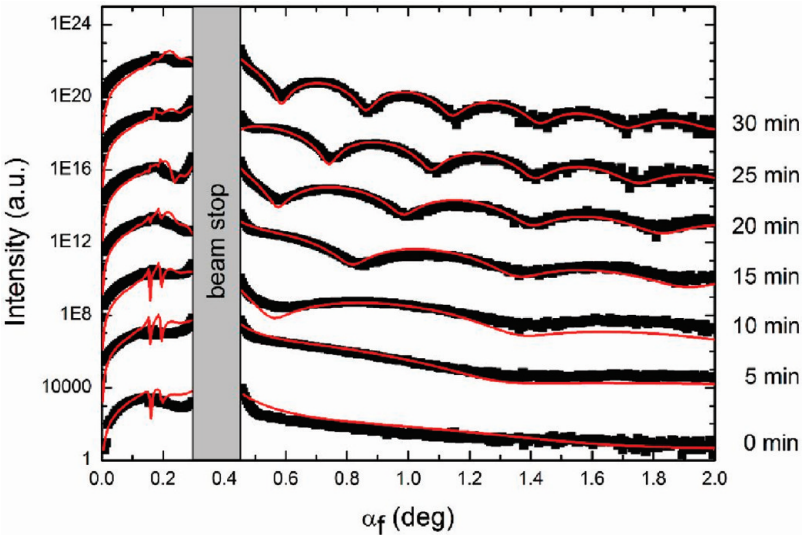

Figure 2. Comparison of selected vertical cuts through the scattering images. The cuts were taken at $\psi = 0°$ and are shifted in intensity for clarity. The solid lines are the cuts through the simulated images.

smooth surface. In the initial stage the amplitude of the maxima is lower than in the final stage, i.e., the relative variations in film thickness become smaller when the film gets thicker and the surface roughness remains low during the whole deposition process.

In contrast to the 2d GISAXS images measured at the inert system gold on PVK during sputter deposition,[30] the scattering images for Al on P3HT do not show any peak-like intensity maxima in the horizontal direction, along the ψ-axis (see figure 1a and 1c). Such side maxima would originate from lateral structures,[49] e.g., Al clusters on P3HT. Even in the images taken during the first minutes of deposition no lateral structure is found, which is seen in the map of the horizontal cuts (Figure 1c). Therefore well-defined in-plane structures in the Al layer are absent and the observed growth process does not proceed by lateral growth and coalescence of spherical clusters. Although the formation of very small aggregates in the initial stage of deposition, which would yield a scattering maximum outside the detected angular range, cannot completely ruled out, the GISAXS measurements clearly show that the growth is different to that of gold on PVK. The surface of the polymer is wetted and already in the initial stage of deposition a continuous layer is formed, which grows in height by adsorption of further impinging Al atoms. Because of the complete coverage of the surface within the deposition of the first atomic layers, no voids or holes form, and the layer structure is homogeneous. Moreover, the Al layer is even long-ranged correlated with the P3HT film surface.

To derive precise values for the Al layer thickness, the 2d GISAXS images were modeled with the IsGISAXS program.[36] A selection of full simulations can be seen in Figure 1a, and the corresponding cuts including the height modulation are shown in Figure 2. A layer stack model, consisting of a glass substrate, a P3HT film with a thickness of 42 nm, and an aluminum layer with variable thickness, was used for modeling. The calculations were performed within the distorted wave Born approximation (DWBA) and by assumption of cylinder-shaped scattering centers. The scattering particles were used to introduce variations in the layer thickness and to describe the amplitude of the modulation. The height of the particles, which approximates the local layer thickness, was distributed with a Gaussian shape. The mean

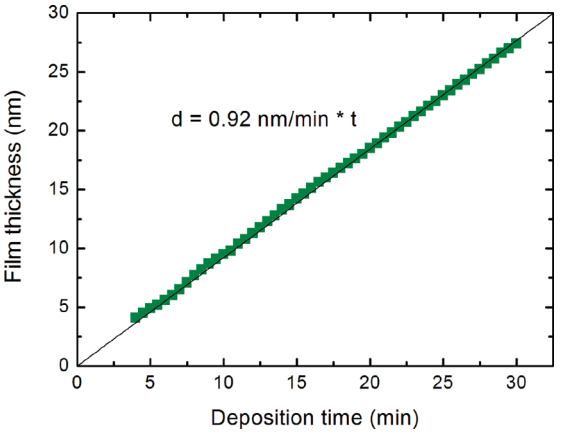

Figure 3. Relation between deposition time and thickness of the Al layer. The solid line is a linear fit to the data. The deposition rate is constant with a value of 0.92 nm/min.

height equals the mean thickness of the layer. From the simulations a relation between deposition time and layer thickness was obtained, which is shown in Figure 3. A linear increase of the Al layer thickness with the deposition time is found, as it is expected for the growth of a smooth homogeneous layer in a two-dimensional growth mode. In particular, no discrepancy between the layer thickness resulting from the deposited amount of material and the observed structural height is visible, as it would be observed in case of a three-dimensional cluster growth mode. Thus the condensation coefficient for the Al atoms on the polymer surface is high already in the initial stage of deposition and nearly all impinging Al atoms are caught, which is indicated by the linear fit passing through the origin at $t = 0$ min. The slope of the fit results in an effective deposition rate of 0.92 nm/min.

To gain further information about the buildup of the Al:P3HT layer system and the structure at the interface, we performed an X-ray reflectivity (XRR) measurement after complete deposition of the Al layer. Because of its sensitivity for small variations in the mass density across the film plane, X-ray reflectivity can detect enrichment layers or inclusions even with only small amounts of incorporated material.[30,50] The measured curve, together with

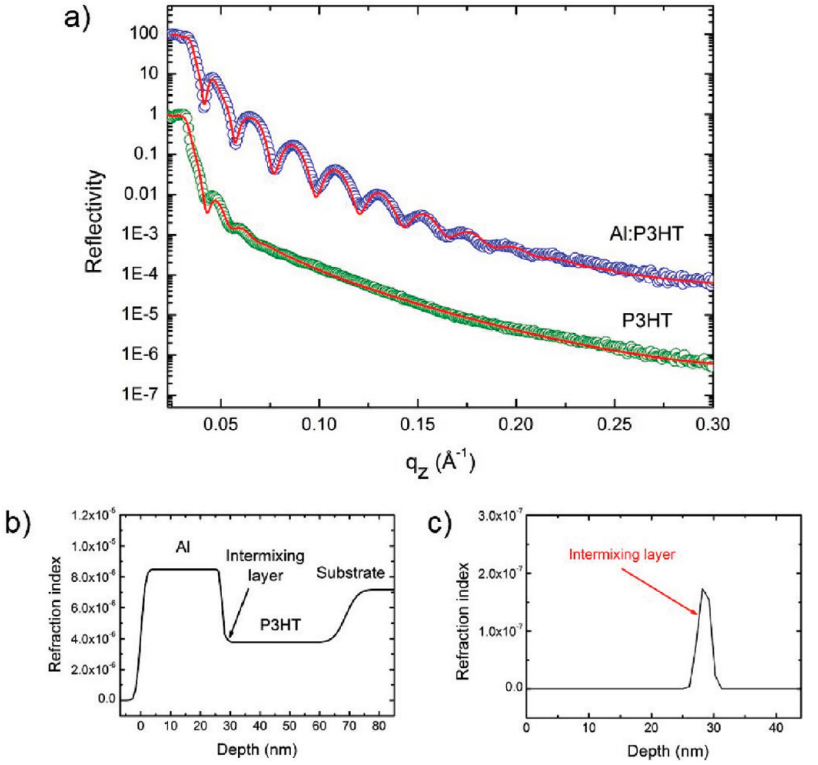

Figure 4. (a) X-ray reflectivity curves of an uncoated P3HT film and the Al:P3HT layer system after complete deposition of the Al contact. The solid lines are fits to the data. (b) Refractive index profile used to fit the data of the Al:P3HT layer system. (c) The subtraction of the profile of a sharp interface with the same surface roughness illustrates the presence of an intermixing layer at the Al:P3HT interface.

the data of an uncoated P3HT film, is shown in Figure 4a. The curve was modeled with a layer stack model, whose refractive index profile is shown in Figure 4b. At the Al:P3HT interface a thin interfacial layer was inserted to model the data correctly. The thickness of this interfacial layer is 2 nm and the refractive index is about 5% above the refractive index value of P3HT. For the surface roughness of the P3HT film, values of 0.5 and 0.6 nm were found in the uncoated and the Al coated film, respectively. Thus the thickness of the interfacial layer is well-distinguished from the roughness of the P3HT film and we attribute the layer to an intermixing zone formed by diffusion of Al atoms into the polymer film. From the measured refractive index value results an Al incorporation in the intermixing layer of 3 wt %. Thus diffusion is only limited and the amount of incorporated Al is small. The included Al atoms are expected also to be chemically bond and complexed with P3HT.[51]

From the refractive index of the top layer (Al layer) results a mass density of 2.75 ± 0.05 g/cm^3. This value is in good agreement with the bulk density of Al (2.71 g/cm^3) and proves the presence of a homogeneous Al layer without voids as it is already concluded from the GISAXS analysis.

The results of the XRR and GISAXS analysis are corroborated by scanning electron microscopy (SEM). Figure 5 shows a SEM image of the Al contact surface after completed sputter deposition. The surface of the 27.7 nm thick Al layer is smooth, without large height deviations. In addition, the SEM image shows a grain structure consisting of small Al grains of approximately 20 nm in size. The grains are rather densely packed but no pronounced order among them is visible. Consequently these grains do not contribute with a structure factor to the GISAXS signal, which is in good agreement with the observed 2d GISAXS patterns.

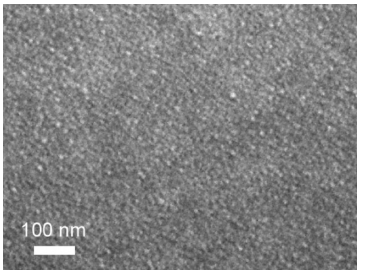

Figure 5. SEM image of the Al surface after deposition of the complete layer.

DISCUSSION

Our experimental findings suggest a growth process that is dominated by a strong chemical interaction at the Al:P3HT interface. The rapid formation of bonds between Al and polymer limits the mobility of the Al atoms on the surface and favors the growth of a smooth layer instead of three-dimensional clusters, in accordance with findings reported for the metallization of metal oxide surfaces.[52,53] Three stages are distinguished in the growth process: (1) surface bonding, (2) agglomeration, and (3) layer growth (see Figure 6). In the first stage, the surface bonding stage, the very first Al atoms impinging on the surface are rapidly bond to the polymer and thus not able to diffuse across the surface to join with other adatoms. Even at low deposits Al atoms are spread uniformly over the surface and the density of nuclei for the layer growth is very high.[53] The growth of three-dimensional cluster structures is suppressed by the low mobility of the adatoms. Simultaneously the probability for desorption is low and condensation already in the initial stage high. With further Al

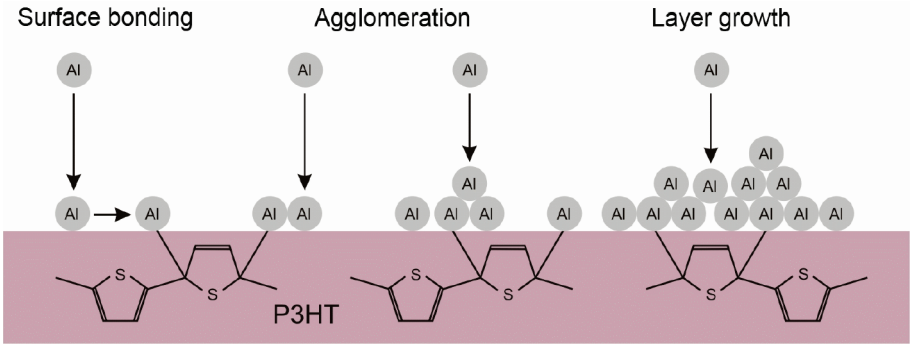

Figure 6. Schematic illustration of the layer growth process. Three stages are distinguished beginning with chemical bonding of single aluminum atoms to the P3HT. Starting from these nuclei the polymer surface is covered rapidly by lateral attachment of further adatoms. Height growth proceeds by deposition of further layers on the first layer.

atoms arriving on the surface the coverage increases and agglomeration sets in, where diffusing adatoms attach laterally to existing nuclei. Because these agglomerates are fixed to the surface, diffusion-enhanced coalescence is not possible and the surface is rapidly covered with an Al layer. Simultaneously, further Al atoms attach on top of this first layer and height growth sets in. With ongoing deposition, more and more Al is deposited and the layer grows continuously in height. Because of the large number of nuclei in the first stage, a crystalline structure develops that consists of a large number of grains with a small size. These grains are densely packed and locally fixed to the polymer substrate, which results in a mass density of the Al layer similar to Al bulk material.

The chemical bonding favors the growth of a dense Al layer without voids and interspaces. Because the interface between the metal and the polymer is not minimized by clustering as in the case of inert systems (e.g., gold on PVK[30]), a high contact area is achieved. Such high contact area is favorable for good adhesion properties of the metal layer on the polymer and avoids delamination of the contact, in particular if it is connected with the formation of an intermixing layer formed by diffusion.[19] But a high contact area also is of relevance for the electric characteristics of the contact, because a large interface allows a charge transfer over a large area and reduces the contact resistance. Thus, a wetting growth mode producing a large interface is preferable compared to a cluster growth mode in order to achieve a contact with beneficial properties.

Because of the low rest gas pressure of 8.4×10^{-8} mbar, we exclude the layer growth process to be initiated by the presence of oxygen, as it was reported for the growth of Al on sexiphyenyl films.[54] At this pressure, only very small amounts of oxygen are present in the deposition chamber, which we assume to be not sufficient to initiate a wetting of the polymer surface. Furthermore, since oxygen cannot be supplied by the P3HT as well, we also exclude the formation of Al_2O_3 during deposition. This is supported by the XRR measurement, which does not show any region with a refractive index higher than that of Al. Because the value of Al_2O_3 is 1.24×10^{-5} and thus well above the value of Al (8.4×10^{-6}), the formation of Al_2O_3 would result in a significant increase in refractive index at the Al:P3HT interface or within the Al layer.

Despite the high reactivity of the Al:P3HT system, diffusion of single Al atoms into the polymer is not completely suppressed. The diffusion process might be promoted by the high energy of the incoming particles and single Al atoms are implanted into the polymer film. Complexed with P3HT molecules these atoms extend the reaction zone into the bulk of the polymer and form a chemically modified layer. Such layers have already been shown to alter the electronic properties of organic layers and to change their charge injection properties.[10]

In general, covalent bonding and the formation of metal−organic complexes is not a peculiarity of the Al:P3HT system. Al is reported also to react with PPV's[51] and small organic semiconducting molecules[10,55] as well as nonconducting polymers.[56−58] Consequently, the growth process on these substrates should be comparable to the growth process on P3HT and result in a similar morphology. Moreover, it is also known that reactive metals grow on oxide surfaces with a high density of nuclei and a full surface coverage even at low deposits.[53] In case of polymers, Demirkan et al. reported about the growth of a thin homogeneous layer of Al on a MEH-PPV surface,[59] and Ho et al. observed less clustering when reactive metals are deposited on polyimide.[58,60] However, in case of low chemical interaction, clustering of the Al on the polymer surface is possible as in the case of inert metals,[54,59] which again shows that reactivity at the interface has a major influence on the growth behavior and the correlating structural properties of the metal layer.

CONCLUSIONS

In summary, we investigated the growth of a metal contact layer on a conductive polymer surface in case of a reactive interaction at the interface. In situ application of GISAXS shows that Al grows on P3HT in a layer growth mode without clustering. The formation of three-dimensional structures is suppressed by the strong chemical interaction of the Al with the P3HT, which bonds the impinging Al atoms to the polymer surface. It is expected that this growth mode is typical for reactive metal−polymer interfaces and advantageous in terms of adhesion and contact resistance.

An XRR measurement shows diffusion of the Al into the P3HT and the formation of an intermixing layer. This layer is only 2 nm thin and has a relative Al incorporation of 3 wt %. Applied in a device the extended zone of complex formation can introduce new states and alter the electronic structure at the interface, which results in modified charge injection properties. Despite the relevance of the system Al:P3HT with respect to application, there are many other metals and polymers used in organic electronics. It remains a promising task for the future to extend this study to other material combinations to gain deeper

inside into the formation of metal−polymer interfaces and the growth of metal coatings on polymer films.

AUTHOR INFORMATION

Corresponding Author
*Phone: +49 (0) 89/289-12451. Fax: +49 (0) 89/289-12473. E-mail: muellerb@ph.tum.de.

ACKNOWLEDGMENT

We thank A. Timmann for assisting the GISAXS experiments and B. Russ and B. Böni for supporting the X-ray reflectivity measurements. Financial support by the Deutsche Forschungsgemeinschaft in the priority program SPP 1181 "Nanomat" (MU1487/5) is gratefully acknowledged. R.M. and V.K. acknowledge financial support by BMBF Project 05KS7W01.

REFERENCES

(1) Burroughes, J. H.; Bradley, J. H.; Brown, A. R.; Marks, R. N.; Mackay, K.; Friend, R. H.; Burns, P. L.; Holmes, A. B. *Nature* **1990**, *347*, 539–541.
(2) Adachi, C.; Baldo, M. A.; Thompson, M. E.; Forrest, S. R. *J. Appl. Phys.* **2001**, *90*, 5048–5051.
(3) Huynh, W. U.; Dittmer, J. J.; Alivisatos, J. P. *Science* **2002**, *295*, 2425–2427.
(4) Padinger, F.; Rittberger, R. S.; Sariciftci, N. S. *Adv. Funct. Mater.* **2003**, *13*, 85–88.
(5) Ma, W.; Yang, C.; Gong, X.; Lee, K.; Heeger, A. J. *Adv. Funct. Mater.* **2005**, *15*, 1617–1622.
(6) Wang, M.; Tang, Q.; An, T.; Xie, F.; Chen, J.; Zheng, S.; Wong, K. Y.; Miao, Q.; Xu, J. *ACS Appl. Mater. Interfaces* **2010**, *2*, 2699–2702.
(7) Wei, Q.; Miyanishi, S.; Tajima, K.; Hashimoto, K. *ACS Appl. Mater. Interfaces* **2009**, *1*, 2660.
(8) Yakimov, A.; Forrest, S. R. *Appl. Phys. Lett.* **2002**, *80*, 1667–1669.
(9) Hadipour, H.; de Boer, B.; Blom, P. W. M. *Adv. Funct. Mater.* **2008**, *18*, 169–181.
(10) Hirose, Y.; Kahn, A.; Aristov, V.; Soukiassian, P.; Bulovic, V.; Forrest, S. R. *Phys. Rev. B* **1996**, *54*, 13748–13758.
(11) Faupel, F.; Willecke, R.; Thran, A. *Mater. Sci. Eng. Rep.* **1998**, *22*, 1–55.
(12) Ettedgui, E.; Razafitrimo, H.; Gao, Y. *Appl. Phys. Lett.* **1995**, *67*, 2705–2707.
(13) Scholz, S.; Huang, Q.; Thomschke, M.; Olthof, S.; Sebastian, P.; Walzer, K.; Oswald, S.; Corten, C.; Kuckling, D. *J. Appl. Phys.* **2008**, *104*, 104502.
(14) Choong, V.; Park, Y.; Gao, Y.; Wehrmeister, T.; Müllen, K.; Hsieh, B. R.; Tang, C. W. *Appl. Phys. Lett.* **1996**, *69*, 1492–1494.
(15) De Puydt, Y.; Bertrand, P.; Lutgen, P. *Surf. Interface Anal.* **1988**, *12*, 486–490.
(16) Silvain, J. F.; Veyrat, A.; Ehrhardt, J. J. *Thin Solid Films* **1992**, *221*, 114–119.
(17) Burkstrand, J. M. *J. Appl. Phys.* **1981**, *52*, 4795–4800.
(18) DeKoven, B. M.; Hagans, P. L. *Appl. Surf. Sci.* **1986**, *27*, 199–213.
(19) *Metallization of Polymers*; Sacher, E.; Pireaux, J.; Kowalczyk, S. P.; Eds.; ACS Symposium Series; American Chemical Society: Washington D.C., 1990.
(20) von Bechtolsheim, C.; Zaporojtchenko, V.; Faupel, F. *Appl. Surf. Sci.* **1999**, *151*, 119–128.
(21) Dannetun, P.; Boman, M.; Stafström, S.; Salaneck, W. R.; Lazzaroni, R.; Fredriksson, C.; Brédas, J. L.; Zamboni, R.; Taliani, C. *J. Chem. Phys.* **1993**, *99*, 664–672.
(22) Becker, H.; Burns, S. E.; Friend, R. H. *Phys. Rev. B* **1997**, *56*, 1893–1905.
(23) Kahn, A.; Koch, N.; Gao, W. *J. Polym. Sci., Part B: Polym. Phys.* **2003**, *41*, 2529–2548.
(24) Hains, A. W.; Ramann, C.; Irwin, M. D.; Liu, J.; Wasielewski, M. R.; Marks, T. J. *ACS Appl. Mater. Interfaces* **2010**, *2*, 175–185.
(25) Strunskus, T.; Kiene, M.; Willecke, R.; Thran, A.; von Bechtolsheim, C.; Faupel, F. *Mater. Corros.* **1998**, *49*, 180–188.
(26) Zaporojtchenko, V.; Zekonyte, J.; Faupel, F. *Nucl. Instrum. Methods Phys. Res., Sect. B* **2007**, *265*, 139–145.
(27) Choi, K. H.; Jeong, J. A.; Kang, J. W.; Kim, D. G.; Kim, J. K.; Na, S. I.; Kim, D. Y.; Kim, S. S.; Kim, H. K. *Sol. Energy Mater. Sol. Cells* **2009**, *93*, 1248–1255.
(28) Bebensee, F.; Zhu, J. F.; Baricuatro, J. H.; Farmer, J. A.; Bai, Y.; Steinruck, H. P.; Campbell, C. T.; Gottfried, J. M. *Langmuir* **2010**, *26*, 9632–9639.
(29) Beyene, H. T.; Chakravadhanula, V. S. K.; Hanisch, C.; Elbahri, M.; Strunskus, T.; Zaporojtchenko, V.; Kienle, L.; Faupel, F. *J. Mater. Sci.* **2010**, *45*, 5865–5871.
(30) Kaune, G.; Ruderer, M. A.; Metwalli, E.; Wang, W.; Couet, S.; Schlage, K.; Röhlsberger, R.; Roth, S. V.; Müller-Buschbaum, P. *ACS Appl. Mater. Interfaces* **2009**, *1*, 353–362.
(31) Müller-Buschbaum, P. *Anal. Bioanal. Chem.* **2003**, *376*, 3–10.
(32) Renaud, G.; Lazzari, R.; Revenant, C.; Barbier, A.; Noblet, M.; Ullrich, O.; Leroy, F.; Jupille, J.; Borensztein, Y.; Henry, C. R.; Deville, J.-P.; Scheurer, F.; Mane-Mane, J.; Fruchart, O. *Science* **2003**, *300*, 1416–1419.
(33) Metwalli, E.; Couet, S.; Schlage, K.; Röhlsberger, R.; Körstgens, V.; Ruderer, M. A.; Wang, W.; Kaune, G.; Roth, S. V.; Müller-Buschbaum, P. *Langmuir* **2008**, *23*, 4265–4272.
(34) Kaune, G.; Memesa, M.; Meier, R.; Ruderer, M. A.; Diethert, A.; Roth, S. V.; D'Acunzi, M.; Gutmann, J. S.; Müller-Buschbaum, P. *ACS Appl. Mater. Interfaces* **2009**, *1*, 2862–2869.
(35) Patel, R. N.; Heitsch, A. T.; Hyun, C.; Smilgies, D.-M.; de Lozanne, A.; Loo, Y.-L.; Korgel, B. A. *ACS Appl. Mater. Interfaces* **2009**, *1*, 1339–1346.
(36) Lazzari, R. *J. Appl. Crystallogr.* **2002**, *35*, 406–421.
(37) Müller-Buschbaum, P.; Hermsdorf, N.; Roth, S. V.; Wiedersich, J.; Cunis, S.; Gehrke, R. *Spectrochim. Acta, Part B* **2004**, *59*, 1789–1797.
(38) Müller-Buschbaum, P. *Eur. Phys. J. E* **2003**, *12*, 443–448.
(39) Couet, S.; Diederich, T.; Schlage, K.; Röhlsberger, R. *Rev. Sci. Instrum.* **2008**, *79*, 093908.
(40) Roth, S. V.; Döhrmann, R.; Dommach, M.; Kuhlmann, M.; Kröger, I.; Gehrke, R.; Walter, H.; Schroer, C.; Lengeler, B.; Müller-Buschbaum, P. *Rev. Sci. Instrum.* **2006**, *77*, 085106.
(41) Yoneda, Y. *Phys. Rev.* **1963**, *131*, 2010–2013.
(42) Sinha, S. K.; Sirota, E. B.; Garoff, S.; Stanley, H. B. *Phys. Rev. B* **1998**, *38*, 2297–2311.
(43) Müller-Buschbaum, P.; Stamm, M. *Macromolecules* **1998**, *31*, 3686–3692.
(44) Müller-Buschbaum, P.; Gutmann, J. S.; Lorenz, C.; Schmitt, T.; Stamm, M. *Macromolecules* **1998**, *31*, 9265–9272.
(45) Müller-Buschbaum, P.; Gutmann, J. S.; Kraus, J.; Walter, H.; Stamm, M. *Macromolecules* **2000**, *33*, 569–576.
(46) Daillant, J.; Bélorgey, O. *J. Chem. Phys.* **1992**, *97*, 5824–5836.
(47) Holý, V.; Baumbach, T. *Phys. Rev. B* **1994**, *49*, 10668–10676.
(48) Wunnicke, O.; Müller-Buschbaum, P.; Wolkenhauer, M.; Lorenz-Haas, C.; Cubitt, R.; Leiner, V.; Stamm, M. *Langmuir* **2003**, *19*, 8511–8520.
(49) Müller-Buschbaum, P.; Cubitt, R.; Petry, W. *Langmuir* **2003**, *19*, 7778–7782.
(50) Diethert, A.; Peykova, Y.; Willenbacher, N.; Müller-Buschbaum, P. *ACS Appl. Mater. Interfaces* **2010**, *2*, 2060–2068.
(51) Salaneck, W. R.; Brédas, J. L. *Adv. Mater.* **1996**, *8*, 48–52.
(52) Campbell, C. T. *Surf. Sci. Rep.* **1997**, *27*, 1–111.
(53) Mattox, D. M. *Thin Solid Films* **1973**, *18*, 173–186.
(54) Ivanco, J.; Winter, B.; Netzer, F. P.; Ramsey, M. G.; Gregoratti, L.; Kiskinova, M. *Appl. Phys. Lett.* **2004**, *85*, 585–587.
(55) Le, Q. T.; Yan, L.; Gao, Y.; Mason, M. G.; Giesen, D. J.; Tang, C. W. *J. Appl. Phys.* **2000**, *87*, 375–379.
(56) DeKoven, M.; Hagans, P. L. *Appl. Surf. Sci.* **1986**, *27*, 199–213.

(57) Bou, M.; Martin, J. M.; Le Mogne, T. *Appl. Surf. Sci.* **1991**, *47*, 149–161.
(58) Ho, P. S.; Hahn, P. O.; Bartha, J. W.; Rubloff, G. W.; LeGoues, F. K.; Silverman, B. D. *J. Vac. Sci. Technol. A* **1985**, *3*, 739–745.
(59) Demirkan, K.; Mathew, A.; Weiland, C.; Reis, M.; Opila, R. L. *J. Appl. Phys.* **2008**, *103*, 034505.
(60) LeGoues, F. K.; Silverman, B. D.; Ho, P. S. *J. Vac. Sci. Technol., A* **1988**, *6*, 2200–2204.